Journal of the Optical Society of America A
OPTICS, IMAGE SCIENCE, AND VISION

Investigation of the moiré patterns of defected radial and circular gratings using the reciprocal vectors approach

MOHAMMAD YEGANEH[1] AND SAIFOLLAH RASOULI[1,2,*]

[1]Department of Physics, Institute for Advanced Studies in Basic Sciences (IASBS), Zanjan 45137-66731, Iran
[2]Optics Research Center, Institute for Advanced Studies in Basic Sciences (IASBS), Zanjan 45137-66731, Iran
*Corresponding author: rasouli@iasbs.ac.ir

Received 2 November 2015; revised 15 January 2016; accepted 20 January 2016; posted 20 January 2016 (Doc. ID 253093); published 25 February 2016

In this work, for the first time to the best of our knowledge, an investigation on the moiré patterns of superimpositions of two radial or two circular gratings consisting of topological defects and their mutual superimpositions with each other, or with linear forked gratings or defected zone plates, is presented. For characterization of the resulting moiré patterns, we use the reciprocal vectors approach. In this approach, by considering local spatial frequencies for the superimposed structures, their reciprocal vectors are determined from the transmission function of the structures. The local reciprocal vector of the resulting moiré pattern at a given point is determined in terms of the local reciprocal vectors of the superimposed structures defined at the same point. In this approach, the topological singularities of the superimposed structures are described by the azimuthal component of the reciprocal vectors. This formulation is very simple, uniform, and comprehensive. In this work, we offer a detailed discussion on the different resulting moiré patterns for the above-mentioned superimpositions and some potential applications of the proposed superimpositions are introduced. In addition, different resulting moiré patterns are simulated.

OCIS codes: (120.4120) Moiré techniques; (110.2650) Fringe analysis; (260.6042) Singular optics; (350.2770) Gratings; (330.7310) Vision.

http://dx.doi.org/10.1364/JOSAA.33.000416

1. INTRODUCTION

Recently, we introduced a new and very simple formulation for analyzing moiré patterns of linear forked gratings (LFGs) and Fresnel zone plates (ZPs) possessing topological defects by the reciprocal vector approach [1]. There, we considered a local spatial frequency for a given periodic or semi-periodic structure and determined its reciprocal vector from the transmission function of the structure. For a given point, the reciprocal vector of the resulting moiré pattern of the superimposition of two periodic structures was expressed in terms of the reciprocal vectors of the superimposed structures for that same point. In this formulation, the topological singularities of the gratings were described by the azimuthal component of the reciprocal vectors used in the sinusoidal amplitude transmission functions of the superimposed structures. We showed that the moiré patterns resulting from the static superposition of different periodic structures possessing topological singularities could be characterized using only the reciprocal vector equation of the resulting moiré patterns. With this formal tool in hand, we approached different kinds of superimposition of LFGs and/or defected zone plates (DZPs). Examples of moiré fringe calculations were presented and images from simulations using MATLAB programming illustrated the calculations. We also offered a detailed discussion based on their theoretical tools. The proposed approach is applicable in the study of the superimposition of a wide class of defected gratings or moiré patterns of semi-periodic structures in which their reciprocal vectors change locally. This approach can also be used in the study of the moiré fringes formed by superimposing linear gratings with slowly varying parameters and moving periodic structures [2,3]. Because of the wide range of applications of radial and circular gratings and their moiré patterns, in this work we apply the proposed approach to the investigation of the moiré patterns resulting from the superimposition of two radial or two circular gratings and their superpositions with each other or with LFGs or DZPs when they possess branching points. The results of these kinds of superpositions are quite interesting and new applications of the moiré technique may be sought in them.

It should be mentioned that in recent decades, the moiré pattern resulting from the superposition of radial and circular

gratings has been used to study different physical effects [4–7] such as in-plane displacement measurements and the strain distribution of soft materials [8], rigid-body displacement measurements [9], and rotational and angular displacement investigations [10–12]. Furthermore, elongated circular gratings have been used for the determinations of both the rigid-body displacement and its direction [13,14]. Also, analytical expressions of the moiré fringes formed by the evolute gratings have been described [15]. Moreover, the circular and radial gratings have also been employed in the visual perception, such as in the illusory motion study and in the vision identification with optical measuring systems [16–18]. In addition, several fantastic illusory motions have also been produced by composition of radially and azimuthally patterns and used in the human vision perception studies [19,20]. On the other hand, in a wide range of applications, the use of radial and circular gratings in the usual interferometry, in Talbot interferometry, and in moiré deflectometry for the measurement of different physical quantities has been reported [21–23]. Examples of more recent applications are the two-step spatial phase-shifting radial shearing interferometry [24] and the volume optical computerized tomography [25,26]. As mentioned above, in this paper we use the proposed reciprocal vectors approach for investigating the moiré patterns of circular and radial gratings possessing topological singularities. In order to present a complete set of moiré patterns illustrating phase singularities of the circular and radial gratings, we introduce new sets of circular and radial gratings consisting of topological defects that we call defected circular gratings (DCGs) and defected radial gratings (DRGs), respectively. Here the topological singularities are also described by the azimuthal component of the reciprocal vectors used in the sinusoidal transmission functions of the gratings. It is worth mentioning that a radial grating intrinsically possessing a singularity at the common center of its rulings extends radially from that point. Hereafter, we refer to the DRG when a radial grating consists of topological defect(s) out of its center. In this work, we present a considerable number of different and interesting moiré patterns of superimpositions of DCGs and DRGs and their mutual superimpositions with each other or with LFGs and DZPs. The formulation of these kinds of moiré patterns is presented in detail by using the reciprocal vectors approach. Details of the calculation are presented and images from simulations using MATLAB programming illustrate the calculations.

Finally, it is worth mentioning that by the composition of different patterns of the defected circular and radial gratings, we have produced different patterns having illusory motions. It seems that these kind of patterns will find a lot of new and fantastic applications in human visual perception. It is known that a significant illusion of motion can be observed in static repeated asymmetric patterns [20]. The main reason for the perception of this kind of illusory motions is related to the small involuntary eye movements during fixation on the patterns. The impact of fixation jitter on the observation or perception of illusory motion for a given pattern differs from one person to another person. We think that by the composition of different repeated defected spiral gratings one can produce new patterns having highly illusory motions and can use them for a more reliable statistical analysis in the perception of illusory motions of people. On the other hand, another reason proposed for the explanation of illusory motion by fast and slow changes over time is the neuronal representation of contrast and luminance of the patterns [20]. In this regard, one can also produce more appearance illusory motions by a collection of defected spiral gratings having different color maps.

2. USE OF THE RECIPROCAL VECTOR APPROACH IN THE MOIRÉ PATTERN FORMULATION

In this section, a brief review of the reciprocal vector approach in the moiré pattern formulation is presented. In this paper, for simplicity, we consider superimposition of amplitude gratings with sinusoidal transmission functions. One can find detailed considerations of the general form of transmission functions of the superimposed gratings in Section 2 of [1] and in [27,28]. The transmission function of a sinusoidal amplitude grating in a general form is given by

$$t(\boldsymbol{\rho}) = \frac{1}{2}\{1 + \cos[\phi(\boldsymbol{\rho})]\}, \tag{1}$$

where ϕ is a scalar function that we call the phase function of the grating, and $\boldsymbol{\rho}$ indicates the position vector on the grating's plane. The phase function changes by a value of 2π from a given ruling to its adjacent ruling on the grating's plane. We introduce a general form for the reciprocal vector of a given grating by $\mathbf{G}(\boldsymbol{\rho}) = \frac{2\pi}{\Lambda(\boldsymbol{\rho})}\widehat{G}$, where $\widehat{G}$ is a unit vector perpendicular to the grating lines and Λ is the spatial period of the grating at a given point having a position vector of $\boldsymbol{\rho}$ from the center of the coordinate system. We have shown that for a given amplitude grating with a sinusoidal transmission function, its local spatial frequency in all coordinate systems is given by

$$\mathbf{G}(\boldsymbol{\rho}) = \pm\nabla\phi(\boldsymbol{\rho}), \tag{2}$$

where the plus and minus signs correspond to the opposite directions of the reciprocal vector of the grating at a given point. Hereafter, for simplicity, we use the plus sign; when we need to use the minus sign, we will state it explicitly. In the superimposition of two gratings, the reciprocal vector of the resulting moiré pattern is given in terms of the reciprocal vectors of the superimposed gratings by [1]

$$\mathbf{G}_{\text{moire}} = \pm\min(\mathbf{G}_1 + \mathbf{G}_2, \mathbf{G}_1 - \mathbf{G}_2), \tag{3}$$

where $\mathbf{G}_1$ and $\mathbf{G}_2$ are the reciprocal vectors of the superimposed gratings. It worth mentioning that both the magnitude and the direction of the reciprocal vector of a grating pattern or a moiré pattern are measurable using Eqs. (2) or (3), respectively.

3. BRIEF REVIEW OF LINEAR FORKED GRATINGS AND DEFECTED ZONE PLATES

A detailed study on the moiré patterns of LFGs and DZPs is presented in [1]. Since in this work we consider mutual superimposition of LFG/DZP and DCG/DRG, a brief review on the presentation of LFGs and DZPs is presented here. The transmission function of an LFG with a sinusoidal amplitude can be written as [1,29]

$$t(x,y)=\frac{1}{2}\left[1+\cos\left(2\pi\frac{x}{\Lambda}-l\varphi\right)\right], \tag{4}$$

where φ denotes the azimuthal angle with respect to the z axis and Λ is the grating's period at a distance away from the dislocation point placed at the center of the coordinate system. The value of l is an integer number, denotes the dislocation of the grating lines, and is called the topological defect number or the defect number of the grating. We call the dislocation point by branch point.

Using Eqs. (2) and (4) the reciprocal vector of a sinusoidal amplitude LFG is given by

$$\mathbf{G}=\frac{2\pi}{\Lambda}\hat{x}-\frac{l}{\rho}\hat{\varphi}, \tag{5}$$

where $\hat{x}$ is the unit vector of the x axis and $\hat{\varphi}$ is the unit vector of the azimuthal angle $\varphi=\tan^{-1}(y/x)$. From the branch point or center of the coordinate system, the radial coordinate is given by $\rho=(x^2+y^2)^{1/2}$. A more general form of LFGs can be found in [1] when they are rotated and displaced in their planes and their branch points are not located at the center of coordinate system.

The transmission function of a DZP with a sinusoidal amplitude is given by [1]

$$t(\boldsymbol{\rho})=\frac{1}{2}\left[1+\cos\left(\frac{\pi\rho^2}{s}-l\varphi'\right)\right], \tag{6}$$

where we named s as the ZP constant. φ' is the azimuthal angle defined at the branch point, and we have

$$\varphi'=\tan^{-1}\left(\frac{y-y_0}{x-x_0}\right),\qquad \rho=(x^2+y^2)^{\frac{1}{2}}, \tag{7}$$

where (x_0,y_0) are the branch point's coordinates in the ZP coordinate system. When the branch point is at the center of a ZP, it is called a spiral ZP (SZP).

For the positive value of the defect number, the branching direction will be along the azimuthal unit vector. Using Eq. (2), the grating's reciprocal vector is given by

$$\mathbf{G}=\frac{2\pi\rho}{s}\hat{\rho}-\frac{l}{\rho'}\hat{\varphi}', \tag{8}$$

where $\hat{\varphi}'$ is unit vector corresponding to the azimuthal coordinate φ' defined from the branch point, and $\rho'=[(x-x_0)^2+(y-y_0)^2]^{1/2}$.

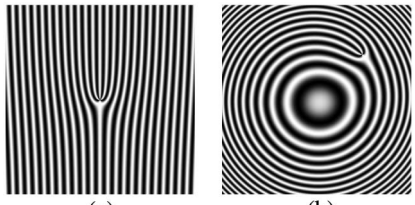

(a) (b)

Fig. 1. (a) A typical sinusoidal LFG pattern with a defect number of $l=+4$. For a grating size of 2.5×2.5 cm^2, the period is $\Lambda=0.1$ cm. (b) A typical DZP with a ZP constant of $s=0.1$ cm^2 and a defect number of $l=3$ in which the branch point's coordinates are $(x_0,y_0)=(0.6,0.6)$ cm. The size of both of patterns is 2.5×2.5 cm^2.

(a) (b) (c)

Fig. 2. (a) A typical sinusoidal CG with period $\Lambda=0.1$ cm, (b) a typical SCG with the same constant and defect number $l=3$, and (c) a typical DCG with the same Λ and l, where the branch point's coordinates are $(x_0,y_0)=(0.6,0.6)$ cm. The size of all the gratings is 2.5 cm × 2.5 cm.

Figure 1(a) shows a typical LFG pattern which has a defect number of 4. In Fig. 1(b), a DZP pattern with a branch point away from the center of the ZP is shown.

4. PRESENTATION OF CIRCULAR GRATINGS CONSISTING OF TOPOLOGICAL DEFECTS

A circular grating (CG) is constructed with a set of concentric rings, where their radial spacing is constant [Fig. 2(a)]. Similar to the DZPs, now we introduce CGs having topological defects and we call these kind of gratings DCGs. The transmission function of a DCG with a sinusoidal amplitude can be written as

$$t(x,y)=\frac{1}{2}\left[1+\cos\left(2\pi\frac{\rho}{\Lambda}-l\varphi'\right)\right], \tag{9}$$

where φ' is the azimuthal angle defined at the branch point, φ' and ρ are given by Eq. (7), and the coordinates of the branch point are (x_0,y_0). Here Λ is the radial period of the grating. When the branch point is at the center of a CG, it is called a spiral CG (SCG). Figure 2(b) shows a typical SCG pattern with a defect number of 3. In Fig. 2(c), a DCG is shown which has a branch point away from the center of the CG. For a positive value of the defect number, the branching direction will be along the azimuthal unit vector. Using Eqs. (2) and (9), the reciprocal vector of the grating is given by

$$\mathbf{G}=\frac{2\pi}{\Lambda}\hat{\rho}-\frac{l}{\rho'}\hat{\varphi}', \tag{10}$$

where $\hat{\varphi}'$ is the unit vector corresponding to the azimuthal coordinate φ' defined by the branch point and $\rho'=[(x-x_0)^2+(y-y_0)^2]^{1/2}$.

5. MOIRÉ PATTERNS OF TWO DEFECTED CIRCULAR GRATINGS

In this section, we consider superposition of two DCGs with radial periods of Λ_1 and Λ_2 and defect numbers of l_1 and l_2 placed at (x_{0_1},y_{0_1}) and (x_{0_2},y_{0_2}), respectively. Using Eqs. (3) and (10), the reciprocal vector of the resulting moiré pattern is obtained as

$$\mathbf{G}_{\text{moire}}=\left(\frac{2\pi}{\Lambda_1}-\frac{2\pi}{\Lambda_2}\right)\hat{\rho}-\left(\frac{l_1}{\rho_1}\hat{\varphi}_1-\frac{l_2}{\rho_2}\hat{\varphi}_2\right), \tag{11}$$

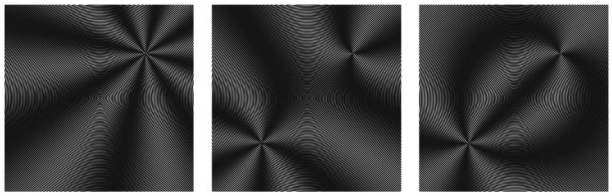

(a) (b) (c)

Fig. 3. Moiré patterns of the superimposition of two DCGs having equal radial periods of $\Lambda = 0.01$ cm. In (a) the branch points of the superimposed gratings coincide at (0.6, 0.6) cm and the defect numbers are $l_1 = 3$ and $l_2 = -5$, respectively. In (b) the branch points are separated with coordinates of $(\pm 0.6, \pm 0.6)$ cm, respectively, and in (c) the defect numbers are changed to $l_1 = 3$ and $l_2 = 5$.

where $\widehat{\varphi}_{1,2}$ are the unit vectors of the azimuthal coordinates $\varphi_{1,2}$ defined on their corresponding branch points, and the radial coordinates $\rho_{1,2}$ are measured from the corresponding branch points $(x_{0_{1,2}}, y_{0_{1,2}})$. In Eq. (11), for equal values of the gratings' periods, the first term vanishes and second term shows two star-like-shaped patterns whose centers are located at the defect points of the superimposed gratings. The number of moiré fringes that come out from these points are equal to $|l_1|$ and $|l_2|$. Similar behaviors have been observed in the superimposition of two LFGs having equal periods (see Fig. 2 of [1]) and in the superimposition of two DZPs having the same ZP constants (see Fig. 7 of [1]). A detailed characterization of this kind of moiré pattern was previously discussed regarding the description of Eq. (15) in [1]. In Fig. 3, three typical moiré patterns of superimposition of two DCGs having equal periods are presented.

Now we consider the superimposition of two DCGs having slightly different radial periods, in which their centers coincide. In this case, according to Eq. (11), the resulting moiré pattern is a magnified DCG with a radial period of $\Lambda_{\text{moire}} = (\Lambda_1\Lambda_2)/|\Lambda_1 - \Lambda_2|$ and its branch points are located at (x_{0_1}, y_{0_1}) and (x_{0_2}, y_{0_2}) coordinates. When $\Lambda_1 > \Lambda_2$, the branching direction corresponding to the first grating's defect point is same as sign of $-l_1$, and the direction of the second branching obeys the sign of $+l_2$. This behavior changes when $\Lambda_2 > \Lambda_1$, as shown in Fig. 4.

(a) (b) (c)

Fig. 4. Moiré patterns of the superimposition of two DCGs having slightly different radial periods and defect numbers of $l_1 = 2$ and $l_2 = 3$. (a) $\Lambda_1 = 0.0041$ cm and $\Lambda_2 = 0.004$ cm and the branch points are located at a common point (0.6, 0.6) cm. (b) The branch points are separated with coordinates of $(\pm 0.6, \pm 0.6)$ cm. (c) The periods of the gratings changed to $\Lambda_1 = 0.004$ cm and $\Lambda_2 = 0.0041$ cm, respectively.

A. Relative Displacements of the Superimposed Gratings

Here we investigate the effect of relative displacements of the superimposed DCGs on the resulting moiré patterns in a case their periods are equal. Similar to DZPs in our previous work [1], here, for a DCG having defect number of l and its center moved to $(\frac{\delta x}{2}, \frac{\delta y}{2})$, we can rewrite its reciprocal vector presented by Eq. (10) as

$$\mathbf{G}_{\frac{\delta x}{2},\frac{\delta y}{2}} = \frac{2\pi}{\Lambda}\widehat{\rho}_1 - \frac{l}{\rho_1'}\widehat{\varphi}_1', \tag{12}$$

where the parameters ρ_1 and ρ_1' and unit vectors $\widehat{\rho}_1$ and $\widehat{\varphi}_1'$ defined as

$$\rho_1 = \left[\left(x - \frac{\delta x}{2}\right)^2 + \left(y - \frac{\delta y}{2}\right)^2\right]^{\frac{1}{2}},$$
$$\rho_1' = \left[\left(x - x_0 - \frac{\delta x}{2}\right)^2 + \left(y - y_0 - \frac{\delta y}{2}\right)^2\right]^{\frac{1}{2}},$$
$$\widehat{\rho}_1 = \frac{1}{\rho_1} \times \left[\left(x - \frac{\delta x}{2}\right)\widehat{x} + \left(y - \frac{\delta y}{2}\right)\widehat{y}\right],$$

and

$$\widehat{\varphi}_1' = \tfrac{1}{\rho_1'} \times \left[-\left(y - y_0 - \tfrac{\delta y}{2}\right)\widehat{x} + \left(x - x_0 - \tfrac{\delta x}{2}\right)\widehat{y}\right].$$

In the superimposing of two DCGs in which their centers are located at $(\mp\frac{\delta x}{2}, \mp\frac{\delta y}{2})$ coordinates, the reciprocal vector of the resulting moiré pattern is given by

$$\mathbf{G}_{\text{moire}} = \frac{2\pi}{\Lambda}(\widehat{\rho}_1 - \widehat{\rho}_2) - \left(\frac{l_1}{\rho_1'}\widehat{\varphi}_1' - \frac{l_2}{\rho_2'}\widehat{\varphi}_2'\right). \tag{13}$$

To illustrate some aspects of the resulting moiré patterns, by considering $\delta x, \delta y \ll \rho$, we expand the first parenthesis and get

$$\widehat{\rho}_1 - \widehat{\rho}_2 \cong \frac{1}{\rho^3}[(y^2\delta x - xy\delta y)\widehat{x} + (x^2\delta y - xy\delta x)\widehat{y}].$$

As a result, the period of the moiré pattern will be $\Lambda_{\text{moire}} = \Lambda\rho^2/(y\delta x - x\delta y)$. In a special case, where we assume $\delta y = 0$, the reciprocal vector of the resulting moiré pattern is

$$\mathbf{G}_{\text{moire}} \cong -\frac{2\pi y\delta x}{\rho^2\Lambda}\widehat{\varphi} - \left(\frac{l_1}{\rho_1'}\widehat{\varphi}_1' - \frac{l_2}{\rho_2'}\widehat{\varphi}_2'\right). \tag{14}$$

In the absence of l_1 and l_2, it indicates a set of radial moiré fringes with a period of $\Lambda_{\text{moire}} = \Lambda\rho^2/y\delta x$ in the azimuthal direction. The number of generated moiré fringes can be determined by a path integral of $\mathbf{G}_{\text{moire}}$ over a simple path surrounding the centers. Here, because $\mathbf{G}_{\text{moire}}$ is an odd function, this integral should be calculated in an interval of $[0, \pi]$ radians and its value multiplied by 2. As a result, we have $N = 4|\delta x|/\Lambda$. Here the integral in a closed path will be equal to zero. This is due to the nature of these moiré lines which do not originate from the phase singularity (see [1]). Depending on the value and sign of the y-component of the position vector, in the superimposition of gratings having defect numbers, different shapes appear around the branch points. If $y > 0$, radially fork-shaped patterns appear and their directions follow the sign of $-l_1$ and $+l_2$, respectively. For $y < 0$, the directions will be changed. The branching direction in branch points in radial shapes will be discussed in Section 8. In a special case, when

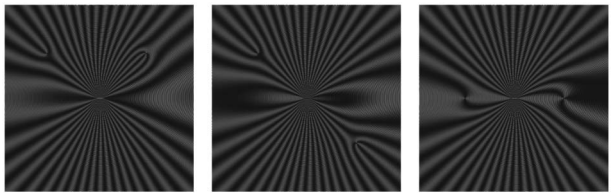

Fig. 5. Moiré patterns of the superimposition of two DCGs having equal periods of $\Lambda = 0.01$ cm and defect numbers of $l_1 = 2$ and $l_2 = 3$, in which their centers separated by $(\delta x, \delta y) = (0.1, 0)$ cm. In (a) the branch points of the gratings are located at $(\mp 0.6, +0.6)$ cm, respectively, in (b) the branch points are changed to the coordinates $(\mp 0.6, \pm 0.6)$ cm, respectively, and in (c) the coordinates are changed to $(\mp 0.6, 0)$ cm, respectively.

$y = 0$, the first expression in Eq. (14) vanishes and star-like patterns with topological defects of $|l_1|$ and $|l_2|$ will appear on the corresponding coordinates. In Fig. 5, three typical moiré patterns of superimposition of two DCGs having equal periods are shown in which there are different separations between their centers.

6. MOIRÉ PATTERNS OF A DCG AND AN LFG

Here we investigate superimposition of a DCG and an LFG. We know that the direction of the reciprocal vector of an LFG is almost constant over the grating's plane, except around the defect point(s). On the other hand, the direction of the reciprocal vector of a DCG is almost in the radial direction. This means that for different values of the azimuthal angle, the angle between the reciprocal vectors of the superimposed gratings is changed. In this case, moiré patterns will appear only around two distinguishable zones in which the directions of the gratings' reciprocal vectors are almost parallel or anti-parallel to each other. The reciprocal vectors of a DCG and an LFG are given by Eqs. (10) and (5), respectively, and they consist of the defect numbers equal to l_1 and l_2 with locations of (x_{0_1}, y_{0_1}) and (x_{0_2}, y_{0_2}), respectively. The spatial periods of the gratings are equal, and the centers of the gratings coincide at the origin of the coordinate system. In this case, the reciprocal vectors of the resulting moiré patterns at the above-mentioned zones are given by

$$\mathbf{G}_{\text{moire}} = \frac{2\pi}{\Lambda}(\widehat{\rho}_1 \pm \widehat{x}) - \left(\frac{l_1}{\rho_1'}\widehat{\varphi}_1' \pm \frac{l_2}{\rho_2}\widehat{\varphi}_2\right), \qquad (15)$$

where the plus and minus signs correspond to the additive and subtractive terms, respectively, of the reciprocal vectors of the superimposed gratings in Eq. (3). Coordinates ρ_1' and ρ_2 and unit vectors $\widehat{\varphi}_1'$ and $\widehat{\varphi}_2$ are defined from the defect points of DCG and LFG, respectively. Unit vector $\widehat{\rho}_1$ is defined from the center of DCG which coincides with the other grating's center. In other word, each of the plus and minus signs in the above equation corresponds to a distinguished moiré pattern appearing at two distinct zones over the superimposition area of the gratings. This is a very interesting case in which both addition and subtraction of the reciprocal vectors of the gratings contributed to the resulting moiré pattern.

Now let us consider places on the superimposed pattern where the azimuthal angle defined from the common center is almost zero. In other words, $\varphi_1 = \theta$ in which $|\theta| \ll 1$. In this case, the minus signs in Eq. (15) should be used and we have $\widehat{\rho}_1 = \cos\theta\widehat{x} + \sin\theta\widehat{y}$. By this consideration, the first set of parentheses in Eq. (15) changes to $(\sin\theta\widehat{y})$. As a result, for $\theta > 0$, if defect points of one or both of the gratings are located in this area ($\varphi_1 \cong 0$), the resulting moiré pattern will have an LFG-shaped pattern having a spatial period of $\frac{\Lambda}{|\sin\theta|}$ and its topological defect will be equal to $+l_1$ or $-l_2$ if the defect point of the DCG or LFG is located at the same point in the area. When both of the defect points take on this area, we will have $\widehat{\varphi}_1' = \widehat{\varphi}_2$ and $\rho_1' = \rho_2$, and the generating LFG pattern will have a topological defect of equal to $(l_1 - l_2)$. For a case in which $\theta < 0$, the signs of the topological defects will be changed. This means that the direction of the branching in the resulting shapes will be changed.

Now we consider an area in which $\varphi_1 = \pi + \theta$, where $|\theta| \ll 1$. In this case, the plus signs in Eq. (15) should be used, and we will have $\widehat{\rho}_1 = -\cos\theta\widehat{x} - \sin\theta\widehat{y}$. The first set of parentheses in Eq. (15) will be equal to $(-\sin\theta\widehat{y})$. For $\theta > 0$, the appearing LFG-shaped pattern in the resulting moiré pattern will have a topological defect equal to $+l_1$ or $+l_2$ if the first or second grating defect point places in this area, respectively. Here its period is also equal to $\frac{\Lambda}{|\sin\theta|}$. In addition, if both of the defect points coincide at the same point in this area, the resulting topological defect will be equal to $(l_1 + l_2)$. Obviously, for $\theta < 0$, the signs of the topological defects will be changed.

If $\varphi_1 = 0$ or $\varphi_1 = \pi$, we will have only star-like-shaped patterns if one or both of the defect points are located in this area. When $\varphi_1 = 0$ and the defect points coincide with each other in this area, the number of moiré fringes originated from this point will be equal to $|l_1 - l_2|$, but if $\varphi_1 = \pi$, the result changes to $|l_1 + l_2|$. Some typical moiré patterns of superimposition of a DCG on an LFG in different cases are shown in Fig. 6.

7. MOIRÉ PATTERNS OF A DCG AND A DZP

In this section, we consider superimposition of a DCG on a DZP having topological defects of l_1 and l_2, respectively. An interesting moiré pattern appears when their centers coincide. In this case, by substituting Eqs. (8) and (10) in Eq. (3), the reciprocal vector of the resulting moiré pattern is given by

$$\mathbf{G}_{\text{moire}} = \left(\frac{2\pi\rho}{s} - \frac{2\pi}{\Lambda}\right)\widehat{\rho} - \left(\frac{l_2}{\rho_2}\widehat{\varphi}_2 - \frac{l_1}{\rho_1}\widehat{\varphi}_1\right), \qquad (16)$$

where $\rho_{1,2}$ and $\widehat{\varphi}_{1,2}$ are radial coordinates and azimuthal unit vectors defined from the branch points of the DCG and DZP, respectively. In the absence of each of the branch points, the area in which the condition of $\rho \approx s/\Lambda$ is satisfied, the first set of parentheses will be approximately equal to zero and a radially parallel kind of moiré fringes will appear. As the radial period of the CG is constant over the grating and period of the ZP is decreasing by increasing ρ, their radial periods to be equal on a ring having radius of $\rho_0 = s/\Lambda$ and the difference of their periods to be very small at the vicinity of the ring. The radial period of the resulting moiré fringes decreases by getting distance from the central moiré ring. We call the widest moiré

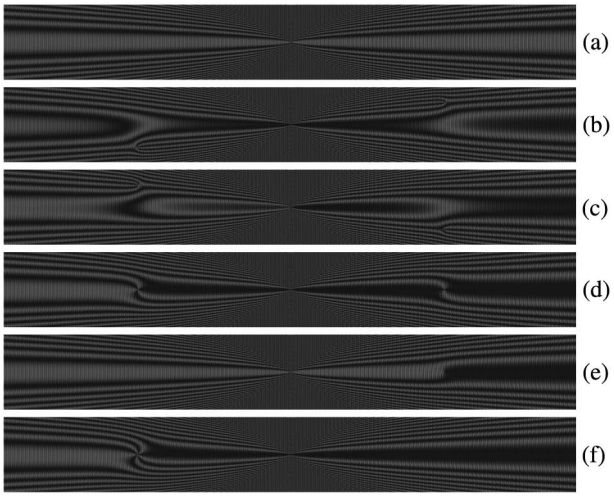

Fig. 6. Moiré patterns of the superimposition of a DCG on an LFG having equal periods of $\Lambda = 0.01$ cm in the case where their centers coincide. The defect numbers of the DCG and LFG in all cases except in (a) are $l_1 = 2$ and $l_2 = 3$, respectively, and the size of the gratings is 7.5×1 cm^2. (a) The defect numbers of two gratings are zero. (b) The defect coordinates of the DCG and LFG are $(x_{0_1}, y_{0_1}) = (2, 0.3)$ cm and $(x_{0_2}, y_{0_2}) = (-2, -0.3)$ cm, respectively ($\theta > 0$ for $\varphi_1 \cong 0$ or π). (c) $(x_{0_1}, y_{0_1}) = (2, -0.3)$ cm and $(x_{0_2}, y_{0_2}) = (-2, 0.3)$ cm, ($\theta < 0$ for $\phi_1 \cong 0$ or π). (d) $(x_{0_1}, y_{0_1}) = (2, 0)$ cm and $(x_{0_2}, y_{0_2}) = (-2, 0)$ cm. (e) Both of the defect points coincide at $(2, 0)$ cm. (f) Both of the defect points coincide at $(-2, 0)$ cm.

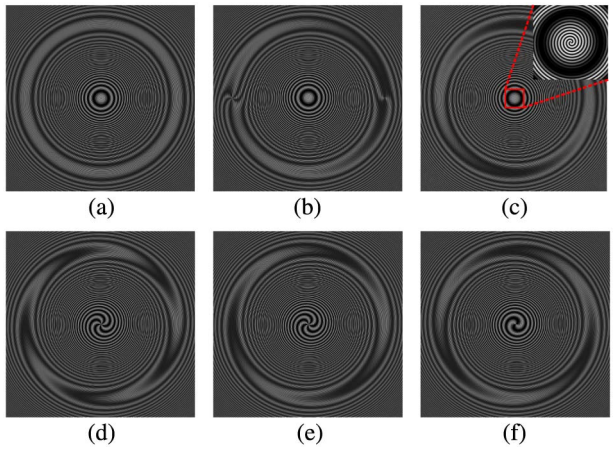

Fig. 7. Moiré patterns of the superimposition of a DCG having $\Lambda = 0.01$ cm and a DZP having $s = 0.01$ cm^2 in the case where their centers coincide. (a) The defect numbers of two gratings are zero. (b) The defect numbers and coordinates of DCG and DZP are $l_1 = 2$ and $l_2 = 5$ and $(x_{0_1}, y_{0_1}) = (1, 0)$ cm and $(x_{0_2}, y_{0_2}) = (-1, 0)$ cm, respectively. (c) $l_1 = 2$ and $l_2 = 0$ and $(x_{0_1}, y_{0_1}) = (0, 0)$ cm. (d) $l_1 = 0$ and $l_2 = 5$ and $(x_{0_2}, y_{0_2}) = (0, 0)$ cm. (e) Both defect points' coordinates are at the common center and $l_1 = 2$ and $l_2 = 5$. (f) Similar to (e), but defect numbers are switched ($l_1 = 5$ and $l_2 = 2$).

fringe the central moiré ring. Here the centers of the resulting radial moiré fringe are same as the centers of the superimposed gratings. The typical shape of the moiré ring is shown in Fig. 7(a). The thickness of the moiré ring can be defined using the fact that changing the phase of the resulting moiré pattern from the center of the moiré ring to the inner or outer limits of the ring should be equal to π on the boundary of the moiré ring. As the reciprocal vectors of the resulting moiré pattern in the inner and outer section of this ring have opposite direction, we consider these two parts, separately. For this reason, we integrate the two sides of Eq. (2) for the reciprocal vector of the moiré ring in Eq. (16), from the middle of the ring to the inner or outer limits of the ring as

$$\pi = \int_{s/\Lambda}^{s/\Lambda \pm \Delta\rho/2} \mathbf{G}_{\text{moire}} . \mathrm{d}\boldsymbol{\rho}. \tag{17}$$

The result indicates that the thickness of the moiré ring is

$$\Delta\rho = 2\sqrt{s}. \tag{18}$$

When one of the branch points is located in the mentioned ring, a SZP pattern appears in the vicinity of the branch point. Due to the changing value of ρ in the vicinity of the branch points in the moiré ring, we define $\rho\widehat{\rho} = \boldsymbol{\rho}'_{1,2} + \rho_{1,2}\widehat{\rho}_{1,2}$, where $\boldsymbol{\rho}'_{1,2}$ are position vectors of the defect points. Because $|\boldsymbol{\rho}'_{1,2}| = s/\Lambda$, Eq. (16) changes to

$$\mathbf{G}_{\text{moire}} \cong \frac{2\pi\rho_{1,2}}{s}\widehat{\rho}_{1,2} - \left(\frac{l_2}{\rho_2}\widehat{\varphi}_2 - \frac{l_1}{\rho_1}\widehat{\varphi}_1\right). \tag{19}$$

By comparison with Eq. (8), we can deduce that the resulting moiré pattern contains two SZP patterns on two defect points with topological defects equal to $-l_1$ and $+l_2$, respectively. This result is observed only on the moiré ring and in the vicinity of the defect points. These features are shown in Fig. 7(b).

For the case in which the branch point of the DCG and the common center of the superimposed gratings coincide, a non-magnified SCG pattern appears around this point with a defect number of $+l_1$, as shown in Fig. 7(c). In a similar case for the DZP, or for both of gratings simultaneously, a nonmagnified SZP with a defect number equal l_2 will appear around the same point [see Figs. 7(d)–7(f)]. These behaviors can be explained as follows. In these cases, the SZP and SCG patterns are not moiré patterns, because these patterns are observed even in the absence of the other grating. However, if branch points of both of gratings lie simultaneously in the common center, because the period of the SZP is larger than the period of the SCG in this area, the dominant pattern will be the SZP pattern shape.

Now let us again to come back to the moiré ring. When one or both of the branch points are taken on the gratings' centers, the transmission function of the moiré pattern in the middle of the moiré ring (at a constant radial coordinate of $\rho_0 = s/\Lambda$) becomes a periodic function of azimuthal coordinate. In other words, a set of secondary moiré fringes appears on the central moiré ring. In this case, from Eq. (16), in the middle of the moiré ring the first set parentheses is equal to zero and we have $\widehat{\varphi}_1 = \widehat{\varphi}_2 = \widehat{\varphi}$ and $\rho_1 = \rho_2 = \rho$. Similar to Eq. (11), for $\Lambda_1 = \Lambda_2$, the number of secondary moiré fringes is obtained from $|l_2 - l_1|$ in the azimuthal direction. By exceeding the value of ρ from ρ_0 to $(\rho_0 + \Delta\rho/2)$, the first set of parentheses in Eq. (16) changes from zero to positive values. As a result, a spiral-shaped pattern is produced in which the direction of its ruling rotation follows the sign of $(l_2 - l_1)$. In the radius between $(\rho_0 - \Delta\rho/2)$ and ρ_0, this behavior will be changed. As

another result, we can deduce a set of shapes similar to arrows appearing on the moiré ring, with the numbers of $|l_2 - l_1|$. The directions of all of these arrows are in $\widehat{\varphi}_0$ when $(l_1 - l_2)$ is positive and for the negative value of $(l_1 - l_2)$ this direction changes to the $-\widehat{\varphi}_0$ direction [Figs. 7(c)–7(f)].

8. PRESENTATION OF RADIAL GRATINGS CONSISTING OF TOPOLOGICAL DEFECTS

A radial grating (RG) is constructed with a set of rulings extended radially from a common center in which the azimuthal angles between the adjacent rulings are equal. As shown in Fig. 8(a), a RG intrinsically consists of a singularity at the center where its rulings extend radially from that point. Like other defected gratings, here we introduce a new set of RGs having additional topological defect(s) located out of their centers, and we call these kind of gratings defected RGs. Hereafter, we call the location of the additional topological defect(s) of a DRG as the defect point(s) of the grating. The transmission function of a DRG with a sinusoidal amplitude can be written as

$$t(x, y) = \frac{1}{2}[1 + \cos(p\varphi - l\varphi')], \tag{20}$$

where p is the total number of the radial rulings of the grating, and φ' is the azimuthal angle defined at the defect point with coordinates of (x_0, y_0). In Figs. 8(b) and 8(c), two typical DRGs having opposite signs of the defect numbers are illustrated. In this case, for the defect point located at the center of the grating, i.e., $\varphi' = \varphi$, the number of rulings comes out from the center of the grating will be equal to $|p - l|$. The reciprocal vector of the grating using Eq. (2) is given by

$$\mathbf{G} = \frac{p}{\rho}\widehat{\varphi} - \frac{l}{\rho'}\widehat{\varphi}', \tag{21}$$

where ρ' and φ' are the radial coordinate and the azimuthal unit vector defined from the defect point, respectively.

9. MOIRÉ PATTERNS OF TWO DEFECTED RADIAL GRATINGS

Now let us investigate several cases of superimposition of two DRGs. For the first case, we assume that the centers of the superimposed DRGs coincide and the corresponding defect points are located at (x_{0_1}, y_{0_1}) and (x_{0_2}, y_{0_2}), respectively. Also, we assume that the defect numbers and the total number of rulings of the DRGs are not identical, i.e., $l_1 \neq l_2$ and $p_1 \neq p_2$. In this case, using Eqs. (2) and (21), the reciprocal vector of the resulting moiré pattern is obtained as

$$\mathbf{G}_{\text{moire}} = \left(\frac{p_1 - p_2}{\rho}\right)\widehat{\varphi} - \left(\frac{l_1}{\rho_1}\widehat{\varphi}_1 - \frac{l_2}{\rho_2}\widehat{\varphi}_2\right). \tag{22}$$

This equation indicates that three star-like-shaped patterns are formed around the common center of the DRGs and around each of the gratings' defect points with defect numbers of $(p_2 - p_1)$, $+l_1$, and $-l_2$, respectively. In other words, the resulting moiré pattern consists of up to three magnified radial fringe patterns: a central branching point located at the center of the gratings and two other branching points at the defect points of the superimposed gratings. In Fig. 9, three different moiré patterns of the superimposition of two DRGs having different ruling numbers and different defect numbers are shown. For the second case, we consider superimposition of two DRGs having equal ruling numbers $(p_1 = p_2 = p)$ and different defect numbers $(l_1 \neq l_2)$, in which their central branching points are separated and located at $(\mp\frac{\delta x}{2}, \mp\frac{\delta y}{2})$, respectively. In this case, the reciprocal vectors of the superimposed gratings are obtained as

$$\mathbf{G}_{\mp\frac{\delta x}{2}, \mp\frac{\delta y}{2}} = \frac{p}{\rho_{1,2}}\widehat{\varphi}_{1,2} - \frac{l_{1,2}}{\rho'_{1,2}}\widehat{\varphi}'_{1,2}, \tag{23}$$

where all coordinates and unit vectors are the same as in Eq. (12) by considering the signs of $\frac{\delta x}{2}$ and $\frac{\delta y}{2}$. The reciprocal vector of the resulting moiré pattern using Eqs. (2) and (23) is given by

$$\mathbf{G}_{\text{moire}} = p\left(\frac{\widehat{\varphi}_1}{\rho_1} - \frac{\widehat{\varphi}_2}{\rho_2}\right) - \left(\frac{l_1}{\rho'_1}\widehat{\varphi}'_1 - \frac{l_2}{\rho'_2}\widehat{\varphi}'_2\right). \tag{24}$$

Now we show some aspects of the resulting moiré patterns. Let us expand the first set of parentheses in the case of $|\delta x|$, $|\delta y| \ll \rho$:

$$\mathbf{G}_{\text{moire}} = \frac{p}{\rho^2}[-\delta y\widehat{x} + \delta x\widehat{y} - 2(\delta x \cos\varphi + \delta y \sin\varphi)\widehat{\varphi}] - \left(\frac{l_1}{\rho'_1}\widehat{\varphi}'_1 - \frac{l_2}{\rho'_2}\widehat{\varphi}'_2\right). \tag{25}$$

In the superimposition of two nondefected radial gratings when their centers are apart, moiré fringes are observed as something like electric field lines of two charges having opposite signs located at the centers of the gratings, as shown in Fig. 10(a). In this case, the reciprocal vector of the resulting moiré pattern along the perpendicular bisector of the line connecting the centers of the gratings, is given by

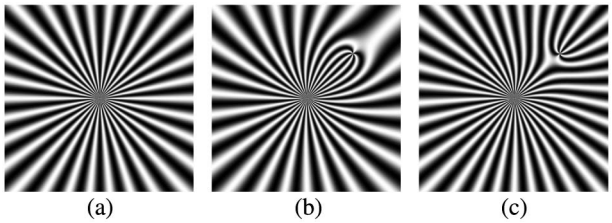

Fig. 8. (a) A typical sinusoidal amplitude RG having a total number of rulings of $p = 30$. (b) A typical DRG with a defect number of $l = 5$ in which the defect point is located at $(x_0, y_0) = (0.6, 0.6)$ cm and in (c) the defect number is changed to $l = -5$. The size of all of the gratings is 2.5 cm × 2.5 cm.

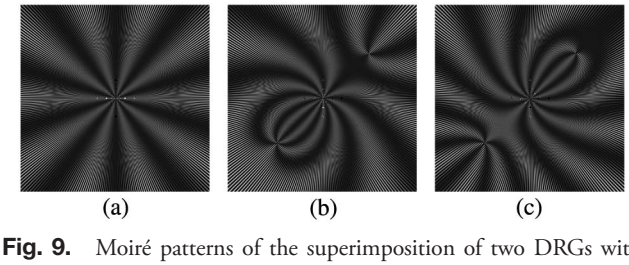

Fig. 9. Moiré patterns of the superimposition of two DRGs with different numbers of rulings. In (a) the defect numbers are zero and the ruling numbers are $p_1 = 300$ and $p_2 = 310$, respectively. In (b) $l_1 = 3$ and $l_2 = 5$ and defect points are located at $(\pm 0.6, \pm 0.6)$ cm, and in (c) the ruling numbers of the gratings are changed to $p_1 = 310$ and $p_2 = 300$.

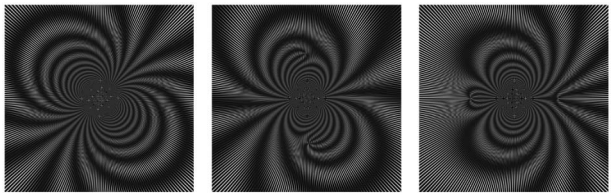

Fig. 10. Moiré patterns of the superimposition of two DRGs, in this case, their centers are separated. Both of the gratings having ruling numbers of $p = 300$. (a) $l_1 = l_2 = 0$ and the centers of the gratings are located at $(\mp 0.025, \mp 0.025)$ cm. (b) $l_1 = 3$ and $l_2 = 5$ and the defect points are located at $(0, \pm 0.6)$ cm and the displacement is in the x direction by $(\mp 0.025, 0)$ cm. (c) $l_1 = 3$ and $l_2 = -5$ and the defect points are located at $(\pm 0.6, 0)$ cm.

$$\mathbf{G}_{\text{moire}} = \frac{p\delta}{\rho^2}(-\sin\theta\hat{x} + \cos\theta\hat{y}), \tag{26}$$

where $\theta = \tan^{-1}(\delta y/\delta x)$ and $\Delta = (\delta x^2 + \delta y^2)^{1/2}$. This equation indicates that over the bisector line, the resulting moiré fringes are parallel to the line connecting the centers of the gratings. The spatial period of the moiré fringes along the bisector changes as a function of distance from the origin of coordinate system, defined at the midway of the centers of the gratings, and is given by $\Lambda = \frac{2\pi\rho^2}{p\Delta}$. For $\delta y = 0$, we have $\Lambda = \frac{2\pi y^2}{p\delta x}$. Now, for simplicity, let us assume that $\delta y = 0$ and focus on the area in which $\varphi = 0, \pi$ in Eq. (25). Therefore, the first part of this equation will be equal to $-\frac{p\delta x}{x^2}\hat{y}$, and if one or both of the singular points is located in this area, we will have one or two fork-shaped patterns around the singular points, in which their defect values and signs follow $-l_1$ and $+l_2$, respectively, if $\delta x > 0$, and for $\delta x < 0$ the signs will be changed. If the singular points lie in other areas, by considering $\delta y = 0$, Eq. (25) changes to

$$\mathbf{G}_{\text{moire}} = -\frac{p\delta x}{\rho^2}\hat{\gamma} - \left(\frac{l_1}{\rho_1'}\hat{\varphi}_1' - \frac{l_2}{\rho_2'}\hat{\varphi}_2'\right), \tag{27}$$

where $\hat{\gamma}$ is a unit vector that corresponds to angle $\gamma = 2\varphi$. This equation indicates that for $\delta x > 0$ in some places in which the singular point is located, the appearing branching pattern will have defect values and signs of $-l_1$ and $+l_2$, respectively. In the investigation of the transmission function of the resulting moiré pattern, a term depending on the 2φ parameter appears in which there is no such dependence in the transmission functions of the superimposed gratings. A detailed analysis of the relation between the value and the sign of the topological charges of the superimposed gratings and the structures of the resulting moiré fringes in which in their phase arguments appear with an additional term with a dependence on 2φ is also an interesting subject. Further investigation of this issue is beyond the scope of the present work. Three typical moiré patterns of the superimposition of two DRGs are shown in Fig. 10.

10. MOIRÉ PATTERN OF A DRG AND AN LFG

In the superimposition of a DRG and an LFG, similar to the case of superimposition of a DCG and an LFG, the direction of the reciprocal vector of the DRG changes by the azimuthal angle, while the direction of same vector of the LFG remains almost unchanged. Therefore, we expect that a moiré pattern appears only in distinct zones over the superimposition area in which the resulting reciprocal vector from the addition and subtraction of the reciprocal vectors of the superimposed gratings are smaller than the gratings' reciprocal vectors. In this case, similar to Section 6, there are two separated zones on the superimposition area: in one zone, the additive kind of moiré pattern is produced, and in the other zone, the subtractive kind of moiré pattern is generated. These moiré patterns correspond to the sum and difference of the reciprocal vectors in Eq. (3). From Eqs. (5) and (21) for the reciprocal vectors of the LFG and DRG, respectively, and considering both the sum and the difference of the reciprocal vectors of the gratings in the generating moiré patterns as shown in Eq. (3), we have

$$\mathbf{G}_{\text{moire}} = \left(\frac{p}{\rho_1}\hat{\varphi}_1 \pm \frac{2\pi}{\Lambda}\hat{x}\right) - \left(\frac{l_1}{\rho_1'}\hat{\varphi}_1' \pm \frac{l_2}{\rho_2}\hat{\varphi}_2\right). \tag{28}$$

Coordinates ρ_1' and ρ_2 and unit vectors $\hat{\varphi}_1'$ and $\hat{\varphi}_2$ are defined from the defect points of the DRG and LFG, respectively. Unit vector $\hat{\varphi}_1$ is defined from the center of the DRG, which is coincident with the other grating's center.

Now we consider two different zones in the superimposition area: the zones in the vicinity of $\varphi_1 \cong \pi/2$ and $\varphi_1 \cong -\pi/2$, respectively. It is worth mentioning that this kind of superimposition around the above-mentioned zones is the same as the superimposition of a linear grating with another linear grating in which the grid's direction of the second one slowly varies from place to place as formulated by an approximated approach in [2]. In the first zone, $\hat{\varphi}_1 = -\cos\theta\hat{x} - \sin\theta\hat{y}$ and $\varphi_1 = \pi/2 + \theta$, where $|\theta| \ll 1$. In the second area, around $\varphi_1 \cong -\pi/2$, we have $\hat{\varphi}_1 = \cos\theta\hat{x} + \sin\theta\hat{y}$ and $\varphi_1 = -\pi/2 + \theta$, where $|\theta| \ll 1$. These assumptions leads to considering the plus sign in Eq. (28) for the first zone and the minus sign for the other one. In the two mentioned zones, around $\rho_1 \cong \frac{p\Lambda}{2\pi}$, we can rewrite Eq. (28) as

$$\mathbf{G}_{\text{moire}} \cong \mp\frac{2\pi\sin\theta}{\Lambda}\hat{y} - \left(\frac{l_1}{\rho_1'}\hat{\varphi}_1' \pm \frac{l_2}{\rho_2}\hat{\varphi}_2\right). \tag{29}$$

If one or both of the defect points of the gratings located in the mentioned zones, in which the azimuthal angle is close to $\pm\pi/2$ and $\rho_1 \cong \frac{p\Lambda}{2\pi}$, this equation indicates an LFG-shaped pattern with a period of $\frac{\Lambda}{\sin\theta}$. The defect numbers and branching directions should be discussed separately for each of the above-mentioned zones. For $\varphi_1 \cong \pi/2$ and the positive value of θ, if the defect point of the DRG or LFG lies in one of the zones, the appearing LFG-shaped patterns have $-l_1$ and $+l_2$ defect numbers, respectively. The negative value of θ changes this result. Obviously, if the two defect points coincide ($\hat{\varphi}_1' = \hat{\varphi}_2$ and $\rho_1' = \rho_2$), the defect number of the resulting LFG-shaped pattern will be $\mp(l_1 + l_2)$ for positive or negative values of θ, respectively. For $\varphi_1 \cong -\pi/2$, the results are slightly different. The defect numbers of the resulting LFG-shaped pattern will have $+l_1$, $-l_2$, and $(l_1 - l_2)$ defect numbers for positive values of θ if the defect points of the DRG, LFG, or both of them are located in the zones, respectively. Similar to the last

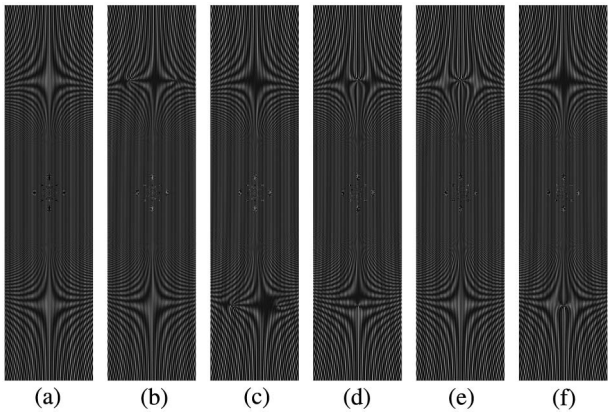

Fig. 11. Moiré patterns of the superimposition of a DRG and an LFG. The number of rulings of the DRG branching from its center is $p = 500$ and the period of the LFG is $\Lambda = 0.0188$ cm, where their spatial periods are equal in $\rho_1 = 1.5$ cm. The size of the gratings is 1.2×5 cm^2. (a) The defect numbers of both of the gratings are zero. (b) The defect numbers of the DRG and LFG are $l_1 = 7$ and $l_2 = 3$, respectively, and the defects' coordinates are $(x_{0_1}, y_{0_1}) = (-0.3, 1.5)$ cm and $(x_{0_2}, y_{0_2}) = (0.3, 1.5)$ cm, respectively, and $(\phi_1 \cong \pi/2)$. (c) The defects' coordinates change to $(x_{0_1}, y_{0_1}) = (-0.3, -1.5)$ cm and $(x_{0_2}, y_{0_2}) = (0.3, -1.5)$ cm and $(\phi_1 \cong -\pi/2)$. (d) $(x_{0_1}, y_{0_1}) = (0, 1.5)$ cm and $(x_{0_2}, y_{0_2}) = (0, -1.5)$ cm $(\theta = 0)$. (e) The defect points coincide at $(0, 1.5)$ cm. (f) The defect points coincide at $(0, -1.5)$ cm.

case, a change in the sign of θ causes a change in the result of the sign.

Now we consider a case in which $\theta = 0$. In this case, the resulting LFG-shaped patterns change to star-like shapes near the defect points in which they are located in the zone of $\varphi_1 = \pm\pi/2$ and $\rho_1 = \frac{p\Lambda}{2\pi}$. The resulting patterns will have $|l_1|$, $|l_2|$, or $|l_1 \pm l_2|$ moiré fringes if the defect point of the DRG, LFG, or both of them is located in the zones, respectively. In Fig. 11, different cases of moiré patterns of a DRG and an LFG are shown.

11. CONCLUSION

In this work, by the reciprocal vectors approach, formulation of moiré patterns in the superimposing of two radial or two circular gratings possessing topological defects and their mutual superimpositions with each other or with linear forked gratings or defected zone plates are presented. For different cases, moiré pattern formulations are investigated and corresponding simulations are presented by MATLAB programming. In addition, a detailed discussion based on the presented theoretical tools for different cases is offered. Similar to the case of linear forked gratings, the presented formulation has potential applications in singular optics measurements. By the superposition of optical fields with the vortices, interference fringes similar to the moiré patterns presented in this work can be obtained [30]. In addition, it seems that these kinds of moiré patterns in an arrangement of gratings in which they are separated, such as in the projection moiré technique like in environmental analyses or in the moiré deflectometry and in the Talbot interferometry, may have a lot of potential applications. It worth mentioning that the optical vortex beam characterizations, such as reconstructing the wavefront and Poynting vector skew angle, have already been done by moiré deflectometry of nondefected linear gratings [31]. We think that the use of defected gratings in moiré deflectometry will pick up its capability in the optical vortex beam characterizations and singular optics measurements. Also, consideration of the dynamic behavior of the presented moiré patterns when the superimposed gratings are moved with respect to each other is another interesting subject. Besides, the presented approach in this paper and the one proposed in [1] can be used in the reformulation and generalization of the moiré fringes formed by superimposing linear gratings with slowly varying parameters has already been presented in [2] by an approximated approach.

Finally, it worth mentioning that we have produced different patterns having illusory motions by the composition of the different patterns of the defected circular and radial gratings. As for the resulting composition patterns, visual illusions can be observed and the observed illusory motions can be changed by changing the defected gratings' parameters. We think that these kinds of patterns will find many applications in the human visual perception.

REFERENCES

1. S. Rasouli and M. Yeganeh, "Formulation of the moiré patterns formed by superimposing of gratings consisting topological defects: moiré technique as a tool in singular optics detections," J. Opt. **17**, 105604 (2015).
2. M. T. Tavassoly and K. Samavati, "Formulation of the moiré fringes formed by superimposing linear gratings with slowly varying parameters," Appl. Opt. **53**, 6612–6618 (2014).
3. S. Rasouli and M. Tavassoly, "Analysis of the moiré pattern of moving periodic structures using reciprocal vector approach," in *Journal of Physics: Conference Series* (IOP Publishing, 2012), Vol. **350**, p. 012032.
4. K. Patorski, *Handbook of the Moiré Fringe Technique* (Elsevier Science, 1993).
5. G. Indebetouw and R. Czarnek, *Selected Papers on Optical Moire and Applications* (Society of Photo Optical, 1992), Vol. **64**.
6. D. Post, B. Han, and P. Ifju, *High Sensitivity Moiré: Experimental Analysis for Mechanics and Materials* (Springer Science & Business Media, 2012).
7. P. Theocaris, *Moiré Fringes in Strain Analysis* (Pergamon, 1969).
8. X. Li, Y. Kang, W. Qiu, Q. Qin, and X. Xiao, "A study on the digital moiré technique with circular and radial gratings," Opt. Lasers Eng. **45**, 783–788 (2007).
9. Y.-C. Park and S.-W. Kim, "Determination of two-dimensional planar displacement by moiré fringes of concentric-circle gratings," Appl. Opt. **33**, 5171–5176 (1994).
10. Y. L. Lay and W. Y. Chen, "Rotation measurement using a circular moiré grating," Opt. Laser Technol. **30**, 539–544 (1998).
11. H. Shang, S. Toh, Y. Fu, C. Quan, and C. J. Tay, "The use of circular optical grating for measuring angular rotation of mirrors," Opt. Lasers Eng. **36**, 487–500 (2001).
12. B. Kim, J. Song, J. Kim, J. Jo, S. Chang, and K. Yuk, "Determination of small angular displacement by moiré fringes of matched radial-parallel gratings," Appl. Opt. **36**, 2848–2855 (1997).
13. J. S. Song, Y. H. Lee, J. H. Jo, S. Chang, and K. C. Yuk, "Moiré patterns of two different elongated circular gratings for the fine visual measurement of linear displacements," Opt. Commun. **154**, 100–108 (1998).
14. B. Kim, K. Yuk, S. Lee, and S. Chang, "Use of a phase type elongated circular grating in Talbot moiré deflectometry," Optik-Int. J. Light Electron Opt. **115**, 121–128 (2004).
15. P. Szwaykowski and K. Patorski, "Moire fringes by evolute gratings," Appl. Opt. **28**, 4679–4681 (1989).

16. H. R. Wilson, R. Blake, and S.-H. Lee, "Dynamics of travelling waves in visual perception," Nature **412**, 907–910 (2001).
17. F. Wilkinson, T. W. James, H. R. Wilson, J. S. Gati, R. S. Menon, and M. A. Goodale, "An fMRI study of the selective activation of human extrastriate form vision areas by radial and concentric gratings," Curr. Biol. **10**, 1455–1458 (2000).
18. M. Ruzzoli, S. Gori, A. Pavan, C. Pirulli, C. A. Marzi, and C. Miniussi, "The neural basis of the enigma illusion: a transcranial magnetic stimulation study," Neuropsychologia **49**, 3648–3655 (2011).
19. H. Ashida, I. Kuriki, I. Murakami, R. Hisakata, and A. Kitaoka, "Direction-specific fMRI adaptation reveals the visual cortical network underlying the 'rotating snakes' illusion," Neuroimage **61**, 1143–1152 (2012).
20. B. T. Backus and İ. Oruç, "Illusory motion from change over time in the response to contrast and luminance," J. Vis. **5**(11), 1055–1069 (2005).
21. O. Bryngdahl, "Radial-and circular-fringe interferograms," J. Opt. Soc. Am. **63**, 1098–1104 (1973).
22. C. L. Koliopoulos, "Radial grating lateral shear heterodyne interferometer," Appl. Opt. **19**, 1523–1528 (1980).
23. D. E. Silva, "Talbot interferometer for radial and lateral derivatives," Appl. Opt. **11**, 2613–2624 (1972).
24. J. Wang, Y. Song, Z.-H. Li, and A.-Z. He, "Two-step spatial phase-shifting radial shearing interferometry with circular gratings," Opt. Lett. **38**, 1116–1118 (2013).
25. J. Wang, Y. Song, Z.-H. Li, and A.-Z. He, "Realization of volume optical computerized tomography by circular gratings," Optik-Int. J. Light Electron. Opt. **124**, 5822–5825 (2013).
26. J. Wang, Y. Song, Z.-H. Li, N. Sun, and A.-Z. He, "Theoretical analysis for moiré effect of circular gratings for volume optical computerized tomography," J. Opt. Soc. Am. A **29**, 1686–1693 (2012).
27. I. Amidror, *The Theory of the Moiré Phenomenon Volume I: Periodic Layers* (Springer-Verlag, 2009).
28. I. Amidror, *The Theory of the Moiré Phenomenon Volume II: Aperiodic Layers* (Springer, 2007).
29. N. Heckenberg, R. McDuff, C. Smith, H. Rubinsztein-Dunlop, and M. Wegener, "Laser beams with phase singularities," Opt. Quantum Electron. **24**, S951–S962 (1992).
30. P. Senthilkumaran, J. Masajada, and S. Sato, "Interferometry with vortices," Int. J. Opt. **2012**, 517591 (2012).
31. M. Yeganeh, S. Rasouli, M. Dashti, S. Slussarenko, E. Santamato, and E. Karimi, "Reconstructing the Poynting vector skew angle and wavefront of optical vortex beams via two-channel moiré deflectometry," Opt. Lett. **38**, 887–889 (2013).